Halide Non-Innocence and Direct Photo-Reduction of Ni(II) Enables Coupling of Aryl Chlorides in Dual Catalytic, Carbon-Heteroatom Bond Forming Reactions

Cameron H. Chrisman[†±], Max Kudisch[†δ±], Katherine O. Puffer[†], Trevor K. Stewart[†], Yisrael M. L. Lamb,[◇] Chern-Hooi Lim[†‡], Randolph Escobar[Δ*], Pall Thordarson[§*], Jeffrey Johannes[Δ*], and Garret M. Miyake[†*]

[†]Department of Chemistry, Colorado State University, Fort Collins, Colorado 80523, United States.

[δ]National Renewable Energy Laboratory, Golden, Colorado 80401, United States.

[‡]New Iridium LLC, Boulder, Colorado 80303, United States.

[§]School of Chemistry, The Australian Centre for Nanomedicine and the UNSW RNA Institute, The University of New South Wales, Sydney, NSW 2052, Australia.

[Δ]Chemistry, Oncology R&D, AstraZeneca, 35 Gatehouse Drive, Waltham, Massachusetts 02451, United States.

[◇]Department of Chemistry and Biochemistry, Fort Lewis College, 1000 Rim Drive, Durango, CO, 81301, United States

[±]These authors contributed equally to this work.

ABSTRACT: Recent mechanistic studies of dual photoredox/Ni-catalyzed, light-driven cross-coupling reactions have found that the photocatalyst (PC) operates through either reductive quenching or energy transfer cycles. To date, reports invoking oxidative quenching cycles are comparatively rare and direct observation of such a quenching event has not been reported. However, when PCs with highly reducing excited states are used (e.g. Ir(ppy)$_3$), photo-reduction of Ni(II) to Ni(I) is thermodynamically feasible. Recently, a unified reaction system using Ir(ppy)$_3$ was developed for forming C–O, C–N, and C–S bonds under the same conditions, a prospect that is challenging with PCs that can photo-oxidize these nucleophiles. Herein, in a detailed mechanistic study of this system, we observe oxidative quenching of the PC (Ir(ppy)$_3$ or a phenoxazine) via nanosecond transient absorption spectroscopy. Speciation studies support that a mixture of Ni-bipyridine complexes form under the reaction conditions, and the rate constant for photoreduction increases when more than one ligand is bound. Oxidative addition of an aryl iodide was observed indirectly via oxidation of the resulting iodide by Ir(IV)(ppy)$_3$. Intriguingly, persistence of the Ir(IV)/Ni(I) ion pair formed in the oxidative quenching step was found to be necessary to simulate the observed kinetics. Both bromide and iodide anions were found to reduce the oxidized form of the PC back to its neutral state. These mechanistic insights inspired the addition of a chloride salt additive, which was found to alter Ni speciation, leading to a 36-fold increase in the initial turnover frequency, enabling the coupling of aryl chlorides.

INTRODUCTION

While light-driven, dual catalytic reaction systems involving a photocatalyst (PC) and a Ni catalyst have emerged as highly promising methods to form C(sp^2)-heteroatom bonds under mild conditions with readily available coupling partners,[1-4] the vast majority of these methods only demonstrate coupling of a single type of nucleophile.[5] In contrast, one of our groups has recently reported a method in which coupling of aryl halides to O, N, or S nucleophiles occurs efficiently without changing the reaction conditions (Fig. 1A).[6] In addition, with a small change in reaction conditions, SCF$_3$ nucleophiles became effective, with 60 examples demonstrated.[7] This universality of a single method is highly desirable for synthetic organic chemistry, especially in medicinal chemistry where these reactions are used at a high frequency.[8-9] In the former system, we proposed a mechanistic hypothesis involving an energy transfer quenching event, supported by literature precedent and a stoichiometric nickel study demonstrating that no added sacrificial oxidant/reductant is needed to promote reactivity — something necessary for photocatalytic cycle turnover in many reductive/oxidative quenching mechanisms.

Recent mechanistic studies[10-11] have disclosed spectroscopic evidence for energy transfer from highly reducing PCs (i.e. Ir(ppy)$_3$ and a phenoxazine (PhenO) PC; ppy = 2-phenylpyridine and PhenO = 3,7-di([1,1'-biphenyl]-4-yl)-10-(naphthalen-1-yl)-10*H*-phenoxazine) to a Ni complex to generate a Ni centered excited state that was crucial for catalysis (Fig. 1B). Based on these reports, we hypothesized that energy transfer would also be the mode of activation of Ni in our unified C─heteroatom coupling system as these same PCs are used. However, the reduction of Ni(II) to Ni(I) by the excited state PC (either Ir(ppy)$_3$ or PhenO; E_{red}* = -1.66 and -1.73 V vs SCE respectively) is thermodynamically feasible based on reported cyclic voltammetry data of relevant nickel bipyridine complexes (E_{red}[Ni(II)/Ni(I)] = -1.0-1.3 V vs SCE).[11-12] Furthermore, in our study with SCF$_3$ nucleophiles, product yield was found to increase as the excited state reduction potential of the PC became more negative, while the triplet energy of the PCs was found to have no correlation with yield. These considerations taken together suggest that the alternate hypothesis of an oxidative quenching cycle (Fig. 1D) should be considered seriously in these systems, motivating a mechanistic study to distinguish between electron transfer and energy transfer as the mode of quenching of the Ir(ppy)$_3$ excited state.

Recently, a number of detailed mechanistic studies have been reported which use a wide range of techniques to elucidate catalytic cycles involving cationic iridium PCs which, as strong photo-oxidants, were reported to participate in reductive quenching cycles[13-15] (Fig. 1C) or energy transfer.[16] Although these reports are highly useful, they provide only limited insight into systems in which highly reducing PCs such as Ir(ppy)$_3$ are used. In contrast, while oxidative quenching cycles (Fig. 1D) have been proposed in the literature occasionally with regards to Ni/PC dual catalytic C─C, C─O, C─N, or C─S bond forming systems, sometimes with computational support,[17-21] experiments capable of distinguishing between oxidative quenching, reductive quenching, and energy transfer (see reviews for relevant spectroscopic and electrochemical methods)[22-24] have not been performed in the study of these systems.

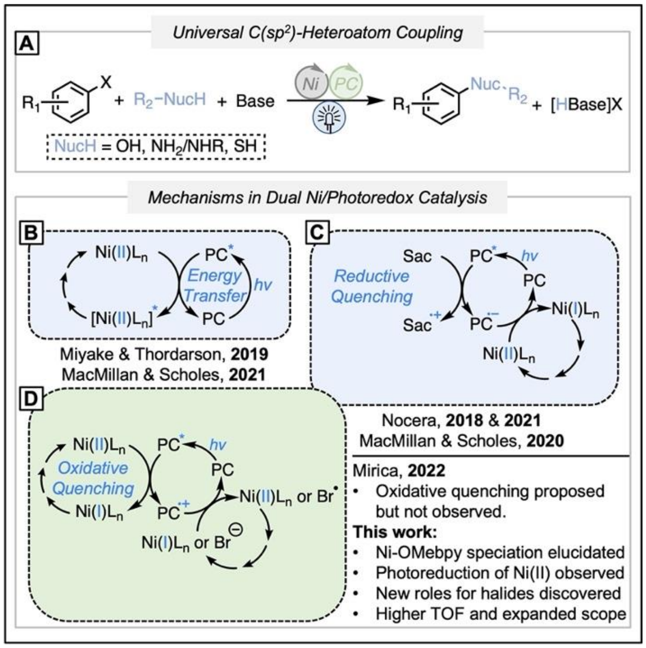

Figure 1. Schemes describing an energy transfer (A),[10-11] reductive quenching (B),[13-15] or oxidative quenching (C)[26] initiated catalytic cycle with examples given that include detailed experimental support for the proposed quenching events. PC = photocatalyst. Sac = sacrificial reductant. TOF = turnover frequency.

Furthermore, computational approaches must explicitly define the species involved, a requirement which can be challenging and even misleading when the precise speciation is unknown due to lack of experimental studies. While the speciation of Ni(II) in the presence of bipyridine type ligands has been studied rigorously,[25] the results are fairly complicated (i.e. slow equilibrium formation of a mixture of species with 0, 1, 2, or 3 bipyridine ligand molecules bound to Ni), and the speciation is expected to vary depending on the particular reaction conditions (e.g. solvent, Ni:ligand molar ratio, ligand identity, and the presence of other reaction components that may ligate Ni). As a result, data concerning the reactivity of specific Ni-bipyridine complexes in dual Ni photocatalysis is severely limited.

More recently, a detailed mechanistic study of a Ni-catalyzed C–O bond formation between alcohols and aryl halides was carried out by Mirica and coworkers.[26] In this work, a tridentate pyridinophane ligand was developed to stabilize Ni(I/III) and utilized to obtain evidence in the form of EPR and stoichiometric studies that supports oxidative addition at Ni(I), binding of the alcohol substrate to Ni(III), deprotonation by the base, and finally reductive elimination to form the aryl ether product. In the case where they use Ir(ppy)$_3$ as a PC, oxidative quenching was proposed on the basis of a redox argument and the observation that product only formed with sufficiently reducing PCs. Although this work is a significant advance in terms of elucidating the reactivity of Ni(I) and Ni(III) intermediates, experimental evidence for the photoreduction of Ni(II) to Ni(I) remains elusive.

Therefore, we undertook a detailed mechanistic study of the system described in Fig. 1A, finding that the photo-reduction of Ni(II) to Ni(I) by the Ir(ppy)$_3$ excited state can be directly observed. Further, we have characterized the nickel-bipyridine complexes formed in this system, studied their reactivity with excited state Ir(ppy)$_3$, found evidence to support oxidative addition of aryl halides at Ni(I) as well as the existence of a 'dark' Ni(I)/Ni(III) cycle, and discovered that bromide and iodide anions are oxidized by Ir(IV) to aid in photocatalyst turnover. Intriguingly, the observed kinetics following the photo-reduction event were best fit with a model invoking a persistent heteronuclear Ni(I)/Ir(IV) ion pair. These findings have enabled us to advance this system and achieve improved reactivity and scope with aryl chloride coupling partners.

RESULTS AND DISCUSSION

Results reported in this section are presented in order of steps in the proposed catalytic cycle, starting with steps that occur prior to light exposure.

Speciation of the Ni Catalyst Prior to Irradiation. Upon mixing all the reaction components, the Ni precatalyst (i.e. $NiBr_2$•glyme) reacts with N,N'-dimethylformamide (DMF) solvent and 4,4'-dimethoxy-2,2'-bipyridine (OMebpy) to form a mixture of Ni-OMebpy complexes (Fig. 2A). We elected to follow the series of dark speciation equilibria through UV-visible spectroscopy, as each complex possesses unique *d-d* absorption bands that can aid in deconvoluting the complex mixtures that result when one mixes $NiBr_2$•glyme with OMebpy in DMF. As such, we conducted a UV-vis titration experiment (Fig. 2B) in which the Ni:OMebpy molar ratio was changed systematically while the solution volume was kept constant (for further details, see SI, Section 2.2).

In DMF, the $NiBr_2$•glyme is proposed to form the octahedral $NiBr_2(DMF)_4$ as the dominant species in solution based on published spectra of related species (see SI, Section 2.1).[10,27] As a Ni:OMebpy ratio of 1:1 is approached, the characteristic broad absorption bands of $NiBr_2(DMF)_4$ with maxima at ~420, ~710, ~760, and ~1250 nm weaken in intensity, while new signals appear with maxima at ~650, ~1020, and ~1120 nm. We assign this spectral change to the first addition of OMebpy to the Ni center to form $NiBr_2(DMF)_2$(OMebpy). Next, as the 1:1 ratio is exceeded and 1:2 is approached, these signals which just formed die away, concomitant with the rise of new signals at ~590, ~800, and ~950 nm that we assign to $NiBr_2(OMebpy)_2$. Finally, signals corresponding to $NiBr_2(OMebpy)_2$ disappear as the ratio of 1:3 is exceeded, and signals with maxima at ~530, ~780, and ~860 nm assigned to $[Ni(OMebpy)_3]Br_2$ appear. Notably, these signals closely match those observed in the literature for $[Ni(bpy)_3]BF_4$ (bpy = 2,2'-bipyridine), supporting our assignment.[25]

To precisely determine the ratio of each species in the Ni-OMebpy mixture, the titration data was fit to four variants (flavors)[28] of a 1:3 (metal:ligand or host:guest) binding model.[10] This fit was performed using a Matlab code based on the analytical solution to the system of equations for the 1:3 equilibria,[10] similar to that described in an NMR study on a 3:1 complexation of a bis-antimony receptor with halide anions.[29] A global analysis[30] using the UV-vis binding isotherms from λ = 450-1200 nm was performed (See SI for details, Section 2.2). Comparing how the variants (flavors) of the 1:3 binding model fitted the data[10, 28, 31] showed that the "full" 1:3 model which assumes both i) cooperativity and ii) that the 1:1, 1:2, and 1:3 stepwise complexes have distinct spectra, gave a significantly better fit to the data.

The full model allowed us not only to extract the stepwise equilibrium binding constants but also the molar absorptivity of each species (Fig. 2C), giving $K_1 = 9.9 * 10^6$ M^{-1}, $K_2 = 2.6 * 10^6$ M^{-1}, and $K_3 = 4.8 * 10^4$ M^{-1} with the corresponding free energies (after correcting for statistical factors) ΔG_1 = –3.9 kcal mol^{-1}, ΔG_2 = –3.8 kcal mol^{-1}, and ΔG_3 = –3.1 kcal mol^{-1}, respectively (Fig. 2C). The increasing ΔG values indicate negative binding cooperativity, or less favorable addition of OMebpy to Ni(II) with each successive association, particularly with the addition of the third ligand (K_3), consistent with the increased steric demand posed by ligation of three OMebpy ligands.

While K_1 agrees well with literature values given for bpy in H_2O and mixed alcohol/aqueous solutions,[25] K_2 and K_3 are several orders of magnitude higher here than in those systems. This difference could be due to the electron rich nature of OMebpy as compared with bpy and/or the difference in binding strength of DMF as compared with protic solvents in terms of coordination to Ni. Given that DMF and other polar, aprotic solvents are often used in dual Ni photocatalysis, we expect these results to be widely applicable.

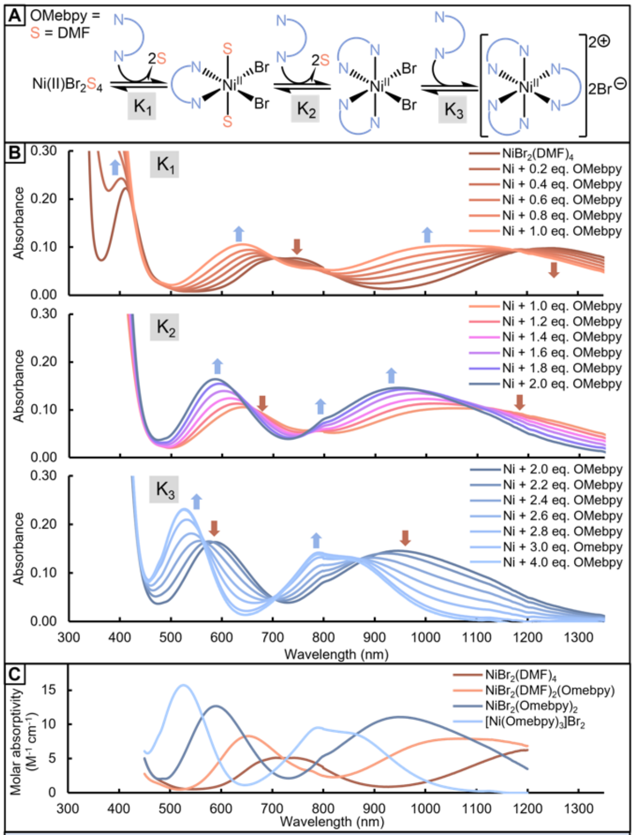

Parameter	K_1 (M^{-1})	K_2 (M^{-1})	K_3 (M^{-1})	ΔG_1[a]	ΔG_2[a]	ΔG_3[a]
Value	$9.9 * 10^6$	$2.6 * 10^6$	$4.8 * 10^4$	–3.9	–3.8	–3.1

Complex	Ratio of Ni to Ligand:	1:1	1:2	1:3
$NiBr_2(DMF)_4$		25.6%	0.4%	0.0%
$NiBr_2(DMF)_2$(Omebpy)		49.1%	10.2%	0.0%
$NiBr_2(OMebpy)_2$		25.1%	78.5%	3.7%
$[Ni(OMebpy)_3]Br_2$		0.2%	10.9%	96.3%

Figure 2. (A) Scheme describing stepwise series of equilibria included in the model. (B) UV-visible spectra of $NiBr_2$•glyme dissolved in DMAc (15 mM) in the presence of increasing molar ratio of OMebpy. (C) Calculated molar absorptivity of each complex as output from the 1:3 Ni:ligand binding model. Spectral region used for fitting = 450-1200 nm. Equilibrium constants, binding energies, and solution compositions are reported. OMebpy = 4-4'-dimethoxy-2-2'-bipyridine. [a]units of kcal mol^{-1}. See SI for details.

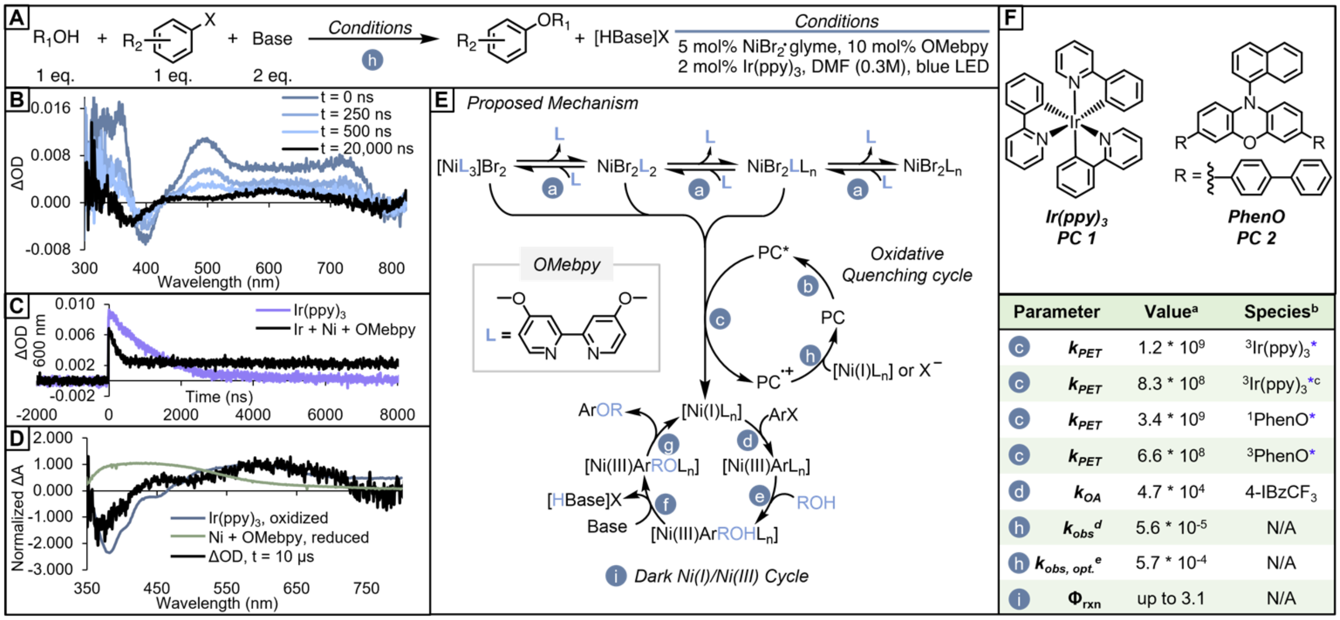

Parameter		Value[a]	Species[b]
c	k_{PET}	$1.2 * 10^9$	^{3}Ir(ppy)$_3$*
c	k_{PET}	$8.3 * 10^8$	^{3}Ir(ppy)$_3$*[c]
c	k_{PET}	$3.4 * 10^9$	^{1}PhenO*
c	k_{PET}	$6.6 * 10^8$	^{3}PhenO*
d	k_{OA}	$4.7 * 10^4$	4-IBzCF$_3$
h	k_{obs}[d]	$5.6 * 10^{-5}$	N/A
h	$k_{obs, opt.}$[e]	$5.7 * 10^{-4}$	N/A
i	Φ_{rxn}	up to 3.1	N/A

Figure 3. (A) Scheme describing net C–O coupling reaction. (B) ns-TA difference spectra at the indicated time delay following the pump pulse (λ = 355 nm, 2-5 mW, ~6 ns pulse width) for a mixture containing Ir(ppy)$_3$ (31.4 µM), NiBr$_2$•glyme (1.5 mM), and OMebpy (3.0 mM, 2 eq. relative to Ni) dissolved in DMF. (C) Kinetic traces of Ir(ppy)$_3$ alone and of the same mixture as in (B) at λ_{probe} = 600 nm. (D) Normalized (to highest peak) difference spectra from spectroelectrochemical experiments in which Ir(ppy)$_3$ was oxidized to Ir(IV) or a mixture of NiBr$_2$•glyme and OMebpy (2 eq. relative to Ni) was reduced electrochemically, overlaid with the t = 10 µs ns-TA spectrum from the same experiment in (B). (E) Generalized mechanism for C–O bond formation. We note that when PC = Ir(ppy)$_3$ the observed kinetics are consistent with a persistent ion pairing mechanism as described below (See Fig. 4 and 5) that differs from this scheme. (F) PCs and structures used in this work. Rate constants measured in this work are reported with lowercase letters indicating the relevant mechanistic steps. Photoinduced electron transfer rates (k_{PET}) were measured via Stern-Volmer quenching studies using ns-TA data, except for the singlet state quenching of PhenO, which used time-correlated single photon counting. [a]Bimolecular rate constants in M^{-1} s^{-1}, pseudo 1st order rate constants in s^{-1}. [b]Species being quenched in Stern-Volmer studies. The quencher was a mixture of NiBr$_2$•glyme and OMebpy (2 eq. relative to Ni) unless otherwise indicated. For k_{OA} the aryl halide was 4-iodobenzotrifluoride. [c]The quencher was a mixture of NiBr$_2$•glyme and OMebpy (1 eq. relative to Ni). [d]Observed pseudo 1st order rate constant from full reaction under standard conditions (See below, Fig.7). [e]Reoptimized conditions, see Fig. 7. See supporting information for additional details.

In addition, the binding model allowed calculation of the exact concentrations of each species at relevant Ni:OMebpy ratios for catalysis (Fig. 2C). Importantly, at the 1:2 ratio used in our system, the dominant species in the Ni-bipyridine mixture is NiBr$_2$(OMebpy)$_2$ at 78.5%, with 10.9% [Ni(OMebpy)$_3$]Br$_2$ and NiBr$_2$(DMF)$_2$(OMebpy) (10.2%), while only 0.4% of the starting NiBr$_2$(DMF)$_4$ remains. Control experiments confirm that the aryl halide, alcohol, and Ir(ppy)$_3$ do not significantly affect the UV-vis signal (See SI, Fig. S9-10) and thus are unlikely to affect the speciation as determined above. Importantly, the alcohol does not bind to the Ni center at this stage, consistent with our hypothesis of transmetalation occurring at Ni(III) as detailed below.

However, K$_2$CO$_3$ causes a blue-shift in the observed signal and increase in absorption at ~530 nm and ~780 nm (Fig. S10) that is consistent with a shift in the equilibria towards increased formation of [Ni(OMebpy)$_3$]Br$_2$. This shift can potentially be explained by carbonate displacing bromide in the outer coordination sphere, inhibiting the dissociation step of K$_3$. If carbonate were bound to Ni(II) in the inner sphere, a change in the UV-vis spectrum would be expected that departs significantly from the signals of the species identified herein. Ni(II) complexes with varying ligation exposed to a carbonate source tend to form multinuclear Ni complexes with bridging carbonate ligands and distinct *d-d* bands in absorption spectra that are not observed here.[32-34]

Mechanistic Hypothesis. With the speciation of the Ni/ligand mixture known, we elected to study the C-O coupling reaction between alcohols and aryl halides as a model system for our mechanistic study (Fig. 3A). We propose a general mechanism, similar to that reported by Mirica and coworkers,[26] that begins with the dark speciation equilibria described in the previous section (Fig. 3E, a). Next, the PC absorbs a photon of light (b) and is oxidatively quenched by one of the Ni species (c) to form a Ni(I) complex that undergoes oxidative addition of the aryl halide (d). Following oxidative addition, the alcohol substrate binds to the Ni center (e) and is deprotonated by the base (f). Finally, the Ni(III) aryl alkoxy complex undergoes reductive elimination to furnish the product (g), closing the Ni(I/III) cycle. The oxidized form of the PC is converted back to the neutral PC through single electron transfer (h) with either a halide anion or the Ni(I) complex, closing both cycles. Steps (d-g) can repeat, constituting a dark Ni cycle (i) that turns over with a frequency distinct from that of the oxidative quenching cycle.

Initiation of Catalysis via Oxidative Quenching. With the possible Ni(II) complexes that may serve as quenchers of the Ir(ppy)$_3$ excited state known, we set out to determine the nature of the reaction between these species. Using nanosecond transient absorption spectroscopy (ns-TA) in combination with electrochemical methods, we engaged in a mechanistic exploration of the quenching step. In the absence of a quencher, the photophysical characteristics of Ir(ppy)$_3$ are well known;

here, we measured the lifetime of the metal-to-ligand charge transfer triplet excited state (^{3}MLCT) at 1.47 ± 0.03 µs at λ_{probe} = 365 nm in degassed DMF under N_2, which agrees well with the reported value of 1.41 ± 0.04 µs.[11] In the presence of a Ni-OMebpy quenching mixture (1:2 OMebpy:Ni), a strong quenching effect is observed, shortening the lifetime to 0.37 ± 0.01 µs at λ_{probe} = 365 nm (Fig. 3C).

Following quenching, signals with maxima at λ = 375 (negative) and λ = 600 nm (positive) are observed to persist well beyond the period of excited state decay and the time window of the experiment (Fig. 3B). To gain insight into the identity of the species produced from the quenching reaction, oxidative spectroelectrochemistry was performed on $Ir(ppy)_3$. The difference spectrum acquired by subtracting spectra before/after electrolysis corresponds to presence of $[Ir(IV)(ppy)_3]^+$ and matches that reported in the literature (Fig. 3D).[11] Importantly, the signals in the spectroelectrochemistry difference spectrum match those in the ns-TA spectrum well, suggesting Ir(IV) is produced in the quenching reaction. The detection of Ir(IV) strongly suggests the production of Ni(I).

To confirm the formation of Ni(I), a second experiment was performed in which a Ni-OMebpy solution (1:2 Ni:OMebpy) was reduced electrochemically while monitoring its UV-vis spectrum. The resulting difference spectrum (Fig. 3D) shows a broad feature with a maximum spanning from ~380-460 nm as the only feature of significance, which is distinct from the spectrum obtained for a related Ni(I) complex produced via cathodic reduction of $NiBr_2$(dtbpy) where dtbpy = 4-4'-di-*tert*-butyl-2-2'-bipyridine (features at λ = ~430 and ~600 nm).[35] This variation is consistent with the fact that the Ni species present in greatest concentration would be distinct in the two cases due to differences in the conditions (mono vs. bis bipyridine complexes, and *tert*-butyl vs. methoxy substitution on the bipyridine).

Interestingly, the observed spectrum can reasonably account for some of the inconsistencies between the ns-TA spectrum and that of Ir(IV) in the spectroelectrochemistry difference spectrum, in particular in the spectral region at λ = ~ 430 nm where Ni(I) shows strongest absorbance. As such, the spectroelectrochemical data supports assignment of the species contributing to the ns-TA signal at t = 10 µs as Ir(IV) and Ni(I). Control experiments support that no species aside from Ni (i.e. free ligand, K_2CO_3, aryl halide, or alcohol) quenches $[Ir(ppy)_3]^*$ significantly (See SI, Section 3.4). In addition, this reduction is electrochemically feasible based on cyclic voltammetry data (E[Ir(III)*/Ir(IV)] = −1.66 V vs. SCE; E[Ni(II)/Ni(I)] = −1.23 V vs. SCE, See SI, Table S5). The PhenO PC is also highly reducing (E[^{1}PhenO*/PhenO$^{\bullet+}$] = −1.73 V vs. SCE),[36] and ns-TA experiments conducted here support that it also engages with Ni-OMebpy complexes via an oxidative quenching pathway (See SI, Section 3.5). This finding raises the broader possibility that any PC with a sufficiently reducing excited state might engage with Ni(II) via oxidative quenching.

Rate of Electron Transfer from PC* to Ni-OMebpy Complexes. Bimolecular rate constants associated with the photoreduction of Ni(II) to Ni(I) by both $Ir(ppy)_3$ and the PhenO PCs (Fig. 3F) were determined by conducting a Stern-Volmer[23] quenching study and monitoring lifetime shortening via ns-TA. Rate constants of $1.2 * 10^9$ and $6.6 * 10^8$ M^{-1} s^{-1} were obtained for the triplet excited states of the Ir and PhenO PCs, respectively. Despite the relatively high triplet quantum yield of 0.91 for PhenO,[37] significant quenching of the PhenO singlet excited state was detectable via time-correlated single photon counting (TCSPC) at total Ni concentrations relevant to catalysis (i.e. 0.2-14.5 mM), giving a rate constant of $3.4 * 10^9$ M^{-1} s^{-1} (Fig. 3F). Recent collaborative work by several of the authors suggests that singlet states are only expected to be significant contributors to catalysis when the quencher is present in sufficiently high concentration.[38]

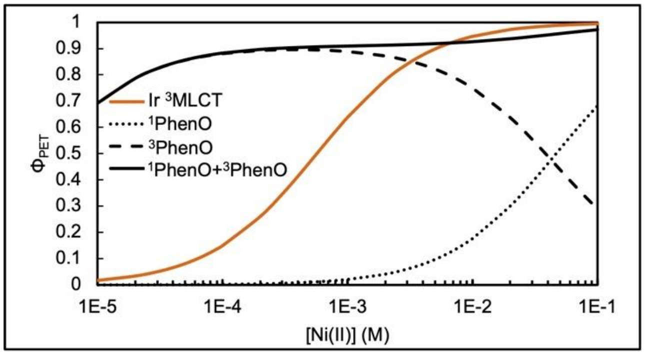

Figure 4. Quantum yield for photoinduced electron transfer for each PC as a function of total Ni(II) complex concentration. Ir ^{3}MLCT refers to the lowest energy triplet metal-to-ligand charge transfer state for $Ir(ppy)_3$. ^{1}PhenO and ^{3}PhenO refer to the lowest-energy singlet and triplet excited states of PhenO, respectively.

Given the known triplet quantum yield of PhenO, we calculated the quantum yield for photoinduced electron transfer, Φ_{PET}, occurring from the singlet (^{1}PhenO) or triplet (^{3}PhenO) excited states and from ^{3}MLCT for $Ir(ppy)_3$ (Fig. 4). At high Ni loadings (e.g. 40 mM Ni), the Φ_{PET} calculated for $Ir(ppy)_3$ is 0.99 (all from the ^{3}MLCT), while for PhenO Φ_{PET} = 0.95 (0.46 from ^{1}PhenO and 0.49 from ^{3}PhenO). Thus, it is expected that $Ir(ppy)_3$ may exhibit slightly better performance at high Ni loadings. The results are consistent with (but may not be the sole contributing factor to) the higher rate of product formation when $Ir(ppy)_3$ is used as opposed to PhenO under the standard Ni loading of 20 mM (See SI for details, Section 6.2). Importantly, ^{1}PhenO state quenching as observed here, despite the relatively few studies elsewhere in dual Ni/photoredox catalysis,[10] should be considered more commonly as a relevant mechanistic pathway when experimental conditions permit (i.e. when organic PCs are used with high quencher concentrations).

In contrast, at low Ni loadings (e.g. 0.2 mM), the calculated quantum yield suggests that PhenO should exceed the performance of $Ir(ppy)_3$ in the oxidative quenching step as Φ_{PET} values for Ir ^{3}MLCT and ^{3}PhenO are 0.26 (all from T_1) and 0.90 (all from T_1), respectively. Indeed, we observed a modest increase in conversion when PhenO was used as compared with the Ir PC at Ni concentrations of 2 mM, 0.2 mM and 0.02 mM (See SI, Section 6.2). Since the overall reaction performance at this Ni loading is poor, we suspect that another step is limiting reaction progress, most likely oxidative addition.

To gain insight into which Ni-OMebpy complex undergoes preferential reduction, dynamic ns-TA quenching experiments were carried out with 1:1, 1:2, or 1:3 ratios of Ni:OMebpy. Under these conditions, the complex present in the highest concentration is $NiBr_2(DMF)_2$(OMebpy), $NiBr_2(OMebpy)_2$, or $[Ni(OMebpy)_3]Br_2$, respectively. Interestingly, the 1:1 mixture was revealed to have a significantly lower rate constant for oxidative quenching than the 1:2 mixture ($8.3 * 10^8$ vs. $1.2 * 10^9$ M^{-1} s^{-1}), while the 1:3 mixture showed nonlinear behavior with similar degree of quenching as compared with the 1:2 mixture (See SI, Fig. S64), suggesting a more complicated mechanism. These results are consistent with the 1:2 Ni:ligand ratio offering the best reaction performance (See SI, Fig. S92).

Oxidative Addition at Ni(I). After formation of Ni(I), it is proposed that oxidative addition (OA) of the aryl halide occurs. Oxidative addition at Ni(I) has been directly observed in recent reports with aryl iodides, with a reduced Ir complex, a radiolytic pulse, or photolysis of an organonickel(II) complex as the source of the Ni(II) to Ni(I) reduction.[13,35,39] Furthermore, oxidative addition of aryl bromides has been followed via EPR in recent work[26] and also through stoichiometric studies of a dimeric Ni(I) complex,[40] both of which support oxidative addition occurring at a monomeric Ni(I) center. Although useful, none of these studies followed Ni(I) generated directly through photoinduced electron transfer as in our approach.

While the Ni(I) signal was too weak to follow via ns-TA here, presumably due to the low molar absorptivity of Ni-OMebpy complexes (~1-15 M^{-1} cm^{-1}), we observed a slow exponential decay of the signal at λ = 600 nm that is predominately due to Ir(IV) on a timescale spanning several hundred µs. Since the signal returns to zero, this decay can be assigned to a back electron transfer reaction (k_{BET} = 5.4 * 10^3 s^{-1}) within the geminate ion pair where Ir(IV) oxidizes Ni(I) to regenerate the neutral pair of species (Fig. 5A). We propose that this [Ir(IV)][Ni(I)] complex remains as a tight ion pair during this step, resulting in the observed unimolecular decay kinetics. It is worth noting that the dominant Ni species here is $[Ni(I)Br_2(OMebpy)_2]^-$ which is well suited to ion pair with $[Ir(ppy)_3]^+$. If a bimolecular BET step is considered instead, a rate constant with a value above the diffusion limit in DMF would be required (See SI, Figure S29).

However, in the presence of aryl iodide (i.e. 4-iodobenzotrifluoride, 4-$IBzCF_3$) the lifetime of the BET decay is shortened significantly (Fig. 5A), indicating a faster recovery of Ir(III). This initially surprising result can be explained through a hypothesis in which Ir(IV) oxidizes OA-generated iodide to produce an iodine radical and recover Ir(III). By variation of the aryl iodide concentration in a Stern-Volmer approach, a rate constant is obtained for the reaction with 4-$IBzCF_3$ of 4.7 * 10^4 M^{-1} s^{-1}, in agreement with previously measured rate constants for oxidative addition with similar aryl iodides at related Ni(I)-bipyridine type complexes (Fig. 5B).[13,35]

In order to explain why the observed kinetics conform to the Stern-Volmer equation, justifying the plot in Fig. 5B, we hypothesize a unimolecular BET event in competition with bimolecular oxidative addition, followed by a fast (> 6.0 * 10^5 s^{-1}, see Supporting Information) unimolecular oxidation of OA-generated iodide by Ir(IV) (See scheme in Fig. 5B). Ir(IV) is thermodynamically capable of oxidizing iodide based on cyclic voltammetry experiments (See SI, Table S5), and we observe byproducts of iodide oxidation in TA experiments in the presence of added NaI (See SI, Fig. S49-50). In sum, our observations are consistent with the hypothesis that OA can be followed indirectly through monitoring the Ir(IV) to Ir(III) turnover kinetics. Furthermore, this observation implicates halide oxidation as a relevant mechanistic step in dual Ni/photoredox catalysis.

In addition, a CV experiment was carried out in which a Ni-OMebpy mixture (1:2, Ni:OMebpy) was reduced alone and in the presence of 4-bromobenzotrifluoride or 4-iodobenzotrifluoride (See SI, Fig. S76). In the presence of either aryl halide, the quasi-reversible reduction becomes irreversible with disappearance of the oxidation waves, consistent with oxidative addition. A greater catalytic current is observed for the aryl iodide as compared with the aryl bromide, suggesting that oxidative addition occurs at a faster rate with that type of substrate, consistent with known OA rates at Ni(I).[35]

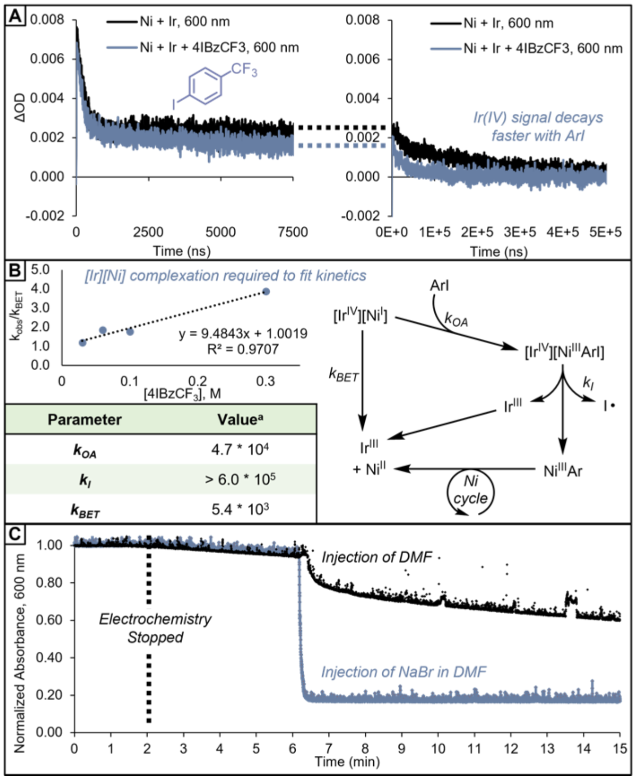

Parameter	Value^a
k_{OA}	4.7 * 10^4
k_I	> 6.0 * 10^5
k_{BET}	5.4 * 10^3

Figure 5. (A) ns-TA kinetic traces (λ_{pump} = 355 nm, 2-5 mW, λ_{probe} = 600 nm) comparing a mixture containing $Ir(ppy)_3$, $NiBr_2$•glyme and OMebpy (2 eq. relative to Ni) with a mixture containing the same components with added 4-iodobenzotrifluoride (0.3 M) over a 7.5 µs time window (left) and a 500 µs time window (right). (B) Plot of k_{obs}/k_{BET} vs. 4-iodobenzotrifluoride concentration (top left). Table of rate constants measured in this segment (bottom left). Scheme defining rate constant. (C) Kinetic spectroelectrochemistry experiment. $Ir(ppy)_3$ was oxidized to completion and the UV-vis signal at λ_{probe} = 600 nm was monitored over time. At t = 2 min, the potentiostat was turned off. At approx. t = 6 min, degassed solutions were injected.

Photocatalyst Regeneration Through Bromide Oxidation. The reaction scheme described above in which iodide liberated through oxidative addition regenerates Ir(III) from Ir(IV) provokes the question as to whether the same chemistry might occur with bromide (either introduced with the $NiBr_2$ source or generated via oxidative addition of an aryl bromide). By CV, the reaction appears to be feasible (See SI, Table S5), although the overpotential is significantly less as compared with iodide. To investigate this potential pathway directly, an experiment was designed in which electrochemically generated Ir(IV) was exposed to bromide after the potentiostat was turned off and the kinetics were followed by UV-vis (Fig. 5C). Importantly, bromide reacted with Ir(IV) as evidenced by a significantly faster decrease in the signal at λ_{probe} = 600 nm as compared with a control run where DMF was injected, causing only a dilution effect. Thus, bromide might serve as a redox mediator to accelerate PC turnover, with the resulting bromine radical deactivating the active Ni(I) complex to form a Ni(II) bromide complex. Other deleterious termination pathways for the bromine radical are certainly possible, for example the radical addition of Br• to a Ni(II) or Ni(III) intermediate, the OMebpy ligand, the substrate, or the nucleophile. We did not detect bromination of the aryl halide substrate or product via ^{19}F NMR (See SI, Fig. S86) and the reaction proceeds to high yield, suggesting a low frequency of termination pathways that lead to Ni catalyst destruction or modification of the coupling partners.

Quantum Yield of Product Formation (Φ_{RXN}). Our proposed mechanism invokes the presence of a dark Ni(I)/Ni(III) cycle (Fig. 3E, i) in which light is only needed for initiation through Ni(II) reduction by the excited state PC to generate Ni(I). After initiation, this cycle can continuously generate product without further light input. One way to support this type of dark cycle is through Φ_{RXN} experiments since a $\Phi_{RXN} > 1$ can only be obtained if product formation occurs independently of a light promoted cycle. We utilized standard ferrioxalate actinometry to measure Φ_{RXN} (See SI, Section 7.1 for further discussion) as a function of light intensity. At the lowest intensity of $I_0 = 5.7 * 10^{-6}$ E L^{-1} s^{-1}, we obtained $\Phi_{RXN} = 3.1$, further supporting our mechanistic hypothesis and ruling out any cycle in which each product formation requires the input of a photon. The fact that Φ_{RXN} is flux-dependent is consistent with a two-cycle mechanism as detailed above in which the PC cycle can operate with a turnover frequency distinct from that of the Ni cycle. Increasing the flux increases the turnover frequency of the PC cycle through increasing the concentration of PC*. Since the total Ni concentration has a fixed maximum, there is a light intensity threshold at which Φ_{PET} begins to decrease with a corresponding increase in Φ for other PC* decay pathways (e.g. internal conversion and radiative decay). At high fluxes beyond this threshold value, Φ_{RXN} decreases below 1 due to the increased prevalence of these PC* decay pathways which do not form product. Broadly, this mechanism has the consequence that the lowest flux at which the rate of product formation is practical for the process will lead to the highest quantum efficiency. Given the mechanistic findings here and in previous sections, we next sought to improve the photocatalytic coupling performance.

Effect of Halide Additives on Reaction Rate. First, we noted a shortcoming of the model system in the use of K_2CO_3 as base in that the reaction is heterogeneous. In order to monitor reaction kinetics with all components present, we replaced K_2CO_3 with 1,8-diazabicyclo(5.4.0)undec-7-ene (DBU) as the base to achieve homogeneous reaction conditions for improved reproducibility. Importantly, we also found that although yields are reproducible in the Hepatochem photoreactor used in our previous work, the kinetics vary drastically by position, likely due to the asymmetric irradiation imposed by the reactor geometry. As such, we conducted kinetic studies in a custom 96-well plate photoreactor (See SI, Fig. S89) which showed much improved reproducibility (% conversion standard deviation = 2.1%, n = 16. See SI, Section 6.1 for details) compared to the Hepatochem (standard deviation = 11%, n = 8).

With the new conditions in hand, we explored the hypothesis that an additional halide source might serve to improve photocatalyst recovery, thereby enabling the Ni(I)/Ni(III) cycle to turn over a greater number of times before deactivation. We screened bromide as an additive with the hypothesis that it would increase the reaction rate through faster catalyst turnover. Indeed, we found that in the coupling between model substrates 4-bromobenzotrifluoride (4-$BrBzCF_3$) and benzyl alcohol (BzOH), tetrabutylammonium bromide (TBABr) increased the conversion by 32% at the 3-hour time point (Fig. 6, entry 2), which is well outside of the well-to-well variability (std. dev. = 2.1%) of our setup. Next, since aryl chlorides are challenging substrates in dual Ni/photoredox methodologies,[41] we tested 4-chlorobenzotrifluoride (4-$ClBzCF_3$) as a substrate with the hypothesis that slower deactivation could improve the coupling with this substrate. As with the aryl bromide, the coupling with 4-$ClBzCF_3$ had higher conversion with bromide additive (entry 4) relative to no additive (entry 3).

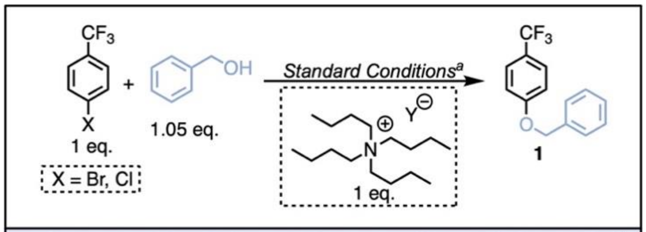

Entry	Time (hr)	X	Y	% Conversion^b
1	3	Br	-	42
2	3	Br	Br	74
3	18	Cl	-	48
4	18	Cl	Br	58
5	18	Cl	I	23
6	18	Cl	Cl	96
7	3	Br	Cl	89

Figure 6. Effect of halide additive on the rate of coupling between 4-$ClBzCF_3$/4-$BrBzCF_3$ and benzyl alcohol. ^{a}Standard Conditions: DMF (0.4 M), $Ir(ppy)_3$ (1 mol%), $NiBr_2 \cdot$glyme (5 mol%), OMebpy (10 mol%), DBU (2 eq.), 35 °C, 445 nm HTE setup. Time and halide additive vary. When used, halide additives at 1 eq. ^{b}Determined via ^{19}F NMR (n = 3).

Since iodide is easier to oxidize than bromide, we next explored increasing the overpotential for Ir(IV) reduction with tetrabutylammonium iodide (TBAI) additive to further increase the rate of catalyst recovery. However, the reaction with TBAI (entry 5) performed worse than no additive. This loss in performance could be due to the formation of $I_2^{\bullet-}$ and I_3^- when iodide is used as an additive. Oxidation of iodide by Ir(IV) is expected to be faster than bromide and the production of $X_2^{\bullet-}$ and X_3^- intermediates is also faster with iodide.[42] The reactivity of these intermediates or the ability of I_3^- and $I_2^{\bullet-}$ to absorb blue light could potentially explain the differences in reactivity between iodide and bromide additives.

While iodide and bromide are thermodynamically capable of reducing Ir(IV) to Ir(III), chloride is outside of the redox window for Ir(IV) reduction (0.98 V vs SCE; See SI, Table S5). Because of this, we hypothesized that using tetrabutylammonium chloride (TBACl) as an additive would give no increase in conversion relative to the additive free reaction. To our surprise, the coupling with TBACl as an additive significantly outperformed the other additive screens, reaching 96% conversion in 18 hours (entry 6). The same increase in reactivity was observed when using TBACl with 4-$BrBzCF_3$ as the substrate (entry 7), giving 89% conversion in 3 hours compared to 42% (entry 1) without additive. It is also worth noting that fluoride gave no conversion in a similar screen (See SI, Section 6.4). To further understand the role of

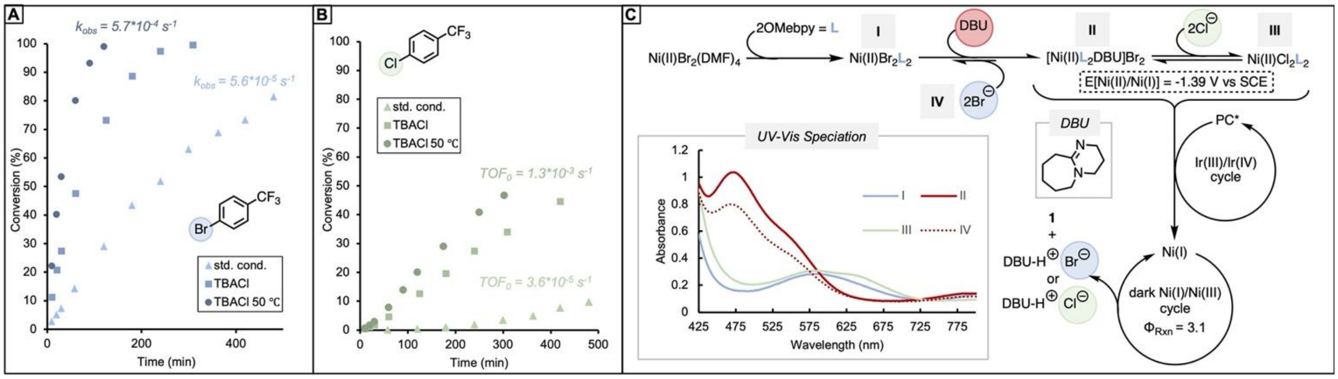

Figure 7. Standard conditions were used. All conversions determined via ^{19}F NMR (n = 3). (A) Kinetics for coupling between 4-$BrBzCF_3$ and benzyl alcohol under standard conditions, with TBACl additive (1 eq.), and at elevated temperatures. (B) Kinetics for coupling between 4-$ClBzCF_3$ and benzyl alcohol under standard conditions, with TBACl additive (1 eq.), and at elevated temperatures. (C) Proposed nickel speciation under standard conditions and modified conditions with halide additives, with UV-vis experiments supporting speciation.

chloride we undertook additional reaction kinetics, UV-vis, and cyclic voltammetry experiments.

Kinetics and Nickel Speciation with Halide Additives. In Rovis and coworker's recent deaminative cross-coupling, chloride significantly improved the system.[43] They hypothesized that one potential role of chloride additive was stopping catalyst death by preventing aggregation. This was supported by the reaction going to high conversion (~90%) with chloride while plateauing at low conversion (~50%) with no additive. However, we did not see this same trend in our kinetics studies. For 4-$BrBzCF_3$, the rate was pseudo-first order with no additive and reached high conversion (Fig. 7A), suggesting that prevention of catalyst death is not the main role of chloride in our system. When running the reaction with 1 eq. TBACl, there was a 4.7-fold increase in k_{obs} and a further 2.2-fold increase at elevated temperature (35 °C vs 50 °C), likely due to faster thermal oxidative addition. Thus, further studies were performed to elucidate the role of the additive.

Running the same kinetics experiments on 4-$ClBzCF_3$ gave more insight into the role of the chloride additive. When the reaction was performed with no external chloride, there was a noticeable induction period (Fig. 7B), suggesting that the byproducts of the aryl chloride coupling are non-innocent. The only byproduct of this coupling is the DBU-HCl salt, which we reasoned could be a source of chloride generated in-situ when no exogenous chloride is present. By saturating the reaction with chloride in the form of TBACl, the coupling with 4-$ClBzCF_3$ displays pseudo-first order kinetics, suggesting that TBACl is involved in the formation of a more active catalyst species. By calculating the initial turnover frequency (TOF_0) for the two cases (added chloride/no added chloride) we found that the species formed with chloride is at least 36-fold more active than the species present with no chloride. Taken together, these results further support chloride as the main contributor to the rate increase and UV-vis studies confirmed a change in nickel speciation that we hypothesize is responsible.

Though nickel speciation was elucidated in experiments above (Fig. 2), these were under the conditions used in our previous methodology study.[6] Since DBU is a known ligand that can change the speciation under our newly developed conditions, we hypothesized that the previously identified Ni(II) complexes may not be the species present in the highest concentration under our new conditions. Indeed, upon adding DBU to a mixture in which the bis-ligated nickel complex is the dominant species (Fig. 7CI to Fig. 7CII), there was a 112 nm hypsochromic shift and an increase in molar absorptivity. The increase in molar absorptivity likely arises from the formation of a 5-coordinate complex from one DBU displacing both bromides to form the complex $[Ni(II)L_2DBU]Br_2$ (See SI for additional discussion).

Next, upon addition of 20 eq. TBACl relative to nickel, we observed a 113 nm bathochromic shift and decrease in molar absorptivity, resembling the spectrum of the $Ni(II)Br_2L_2$ complex (Fig. 7CIII). This complex was confirmed to be $Ni(II)Cl_2L_2$ by comparing the diffuse reflectance spectrum of the isolated species to the complex formed directly from $NiCl_2$•glyme and 2 eq. OMebpy (See SI, Fig. S13), with matching features and a reflectance maximum at ~630 nm. Additionally, the formation of $Ni(II)Cl_2L_2$ as a more active catalyst was further supported by an increase in conversion when $NiCl_2$•glyme was used in place of $NiBr_2$•glyme in the absence of additive (See SI, Section 6.5), though $NiBr_2$•glyme with TBACl still gave the best conversion. Lastly, upon addition of TBABr to $[Ni(II)L_2DBU]Br_2$ we observed only a very minor change in the spectral features (Figure 7CIV), and the formation of a small amount of $Ni(II)Br_2L_2$ was confirmed in the normalized difference spectrum (See SI, Fig. S12). To understand why $Ni(II)Cl_2L_2$ is responsible for the observed increase in reactivity, we next turned to studying the redox properties of the above species.

Recent work found a similar change in speciation upon addition of chloride and a concomitant decrease in the Ni(I)/Ni(II) redox couple of 0.15 V.[44] The authors hypothesized that lowering the reduction potential of Ni(II) increases the overall reaction rate. However, we found that the Ni(I)/Ni(II) couple was identical for $[Ni(II)L_2DBU]Br_2$ and $Ni(II)Cl_2L_2$ (E[Ni(II)/Ni(I)] = –1.39 V vs SCE), meaning a redox argument is not sufficient for explaining the difference in reactivity. Since the redox couples are identical, we are currently focusing our efforts on rates of other steps in the catalytic cycle (e.g. back electron transfer, oxidative addition, and transmetalation) to explain the increase in reactivity with chloride additive.

Expanded Reaction Scope. Based on the faster rate of product formation as quantified by an increase in k_{obs} and TOF_o with DBU and added chloride, as well as the high conversion we observed with 4-$ClBzCF_3$, we explored the scope of the reaction with other challenging aryl halides and nucleophiles (Fig. 8). First, under our newly developed conditions we were able to obtain model compound 1 in 74% isolated yield. Though a similar coupling product was obtained in our previous work

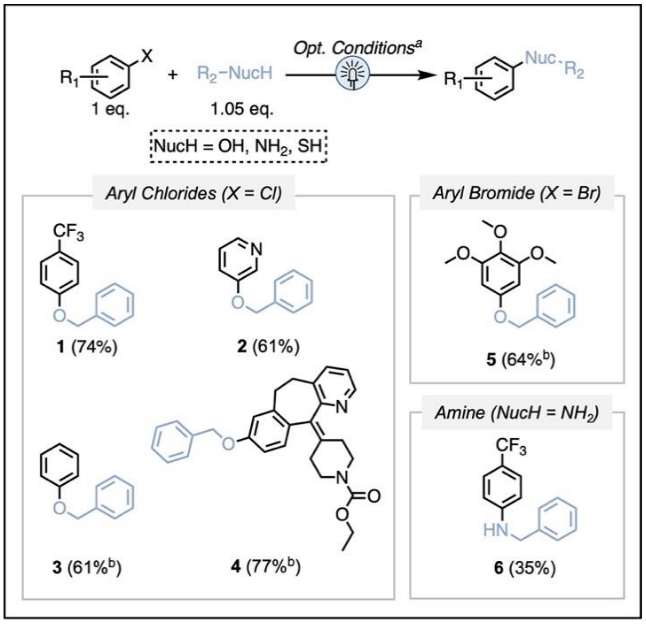

Figure 8. Aryl halide and nucleophile scope with optimized conditions. [a]Optimized conditions: aryl halide (1 mmol), nucleophile (1.05 mmol), Ir(ppy)$_3$ (0.01 mmol), DBU (2 mmol), NiBr$_2$•glyme (0.05 mmol), OMebpy (0.1 mmol), DMF (0.4 M), 440 nm Hepatochem setup, 50 °C, 18 hr. [b]Run at 70 °C.

in 64% isolated yield, these conditions gave highly variable results in the formation of 1, with NMR yields ranging from 9-30% herein. We believe this variability could arise from differing amounts of chloride contamination in the batches of carbonate that were used (See SI, Section 6.7 for further discussion). Next, we were able to couple electron deficient 3-chloropyridine and benzyl alcohol to give product 2 in 61% yield. We then investigated the ability of our system to enable coupling with electronically neutral aryl chlorides and successfully isolated the products from the coupling with chlorobenzene (3, 61%) and loratadine (4, 77%), albeit at elevated temperature (70 °C).

The coupling with loratadine demonstrates the applicability of our method in late-stage functionalization and it was particularly encouraging that we saw no transesterification due to the mild nature of our conditions. Though electron rich aryl chlorides, such as *N*-Boc-5-chloroindole, were unsuccessful under our conditions (<10% crude yield), likely due to slow oxidative addition, we were able to couple the highly electron rich 5-bromo-1,2,3-trimethoxybenzene to yield 5 in 64% yield. Lastly, the coupling with benzyl amine instead of benzyl alcohol to yield 6 (35%) demonstrates that our new conditions do not prevent reactivity with other nucleophiles. However, the coupling with benzyl mercaptan was unsuccessful, which we believe arises from thiol deprotonation by DBU and the resulting thiolate altering the Ni speciation. Though the new conditions inhibited reactivity with thiols, the ability to turn on chloride reactivity and maintain amine reactivity demonstrates how utilizing mechanistic insights can improve reaction scope in dual photoredox/Ni catalyzed couplings.

CONCLUSION

In summary, through spectroscopic and electrochemical studies, this work provides mechanistic insights into an oxidative quenching pathway in dual Ni/PC catalyzed C-X bond forming reactions. Specifically, oxidative quenching of the PC excited state to form a Ni(I) complex was observed spectroscopically, as well as the subsequent oxidative addition of an aryl iodide at Ni(I) and consequent oxidation of iodide by Ir(IV). Interestingly, persistent tight ion pairing in a series of [Ir][Ni] complexes was invoked to simulate the observed oxidative addition kinetics. Future studies ought to confirm or falsify this deduction by utilizing experimental methods capable of distinguishing tight and solvent separated ion pairs formed as a result of PET, such as time resolved dielectric loss spectroscopy.[45]

Additionally, turnover of the Ir(IV) species to recover Ir(III) by halides (Br-, I-) or Ni(I) was confirmed with spectroelectrochemistry and ns-TA experiments. A new role of chloride additive was discovered in binding to the Ni center to displace DBU, forming an octahedral Ni chloride species which led to a significant increase in reactivity to enable coupling of electron deficient/neutral aryl chlorides and highly electron rich aryl bromides. Notably, a novel loratadine derivative was synthesized with the reoptimized conditions, supporting the potential utility of the method discovered through the mechanistic studies herein for late-stage functionalization of medicinally relevant compounds.

ASSOCIATED CONTENT

Supporting Information. The supporting information consists of transient absorption spectroscopic data, cyclic voltammetry data, spectroelectrochemistry data, UV-visible spectroscopy and data analysis, and details regarding C–O cross coupling reaction procedures and product characterization. This material is available free of charge via the Internet at http://pubs.acs.org.

AUTHOR INFORMATION

Corresponding Author

*garret.miyake@colostate.edu
*p.thordarson@unsw.edu.au
*Jeffrey.Johannes@astrazeneca.com
*randolph.escobar@astrazeneca.com

Notes

The authors declare no competing financial interests.

ACKNOWLEDGMENT

This work was supported by Colorado State University, the National Institutes of Health (Award Number R35GM119702) and the Australian Research Council (Discovery Grant DP220101847). The content is solely the responsibility of the authors and does not necessarily represent the official views of the above institutions.

ABBREVIATIONS

PC, photocatalyst; TA, transient absorption; CV, cyclic voltammetry; PET, photoinduced electron transfer; k_q, quenching rate constant; DBU, 1,8-diazabicyclo[5.4.0]undec-7-ene; 4-ClBzCF$_3$, 4-chlorobenzotrifluoride; 4-BrBzCF$_3$, 4-bromobenzotrifluoride; DMF, *N*,*N*-dimethylformamide; TBACl, tetrabutylammonium chloride; TBABr, tetrabutylammonium bromide; TBAI, tetrabutylammonium iodide; TBAF, tetrabutylammonium fluoride; OMebpy, 4-4’-dimethoxy-2-2’-bipyridine; PhenO, 3,7-di([1,1'-biphenyl]-4-yl)-10-(naphthalen-1-yl)-10*H*-phenoxazine.

REFERENCES

(1) Oderinde, M. S.; Jones, N. H.; Juneau, A.; Frenette, M.; Aquila, B.; Tentarelli, S.; Robbins, D. W.; Johannes, J. W., Highly Chemoselective Iridium Photoredox and Nickel Catalysis for the Cross-Coupling of Primary Aryl Amines with Aryl Halides. *Angewandte Chemie International Edition* **2016,** *55* (42), 13219-13223.

(2) Oderinde, M. S.; Frenette, M.; Robbins, D. W.; Aquila, B.; Johannes, J. W., Photoredox Mediated Nickel Catalyzed Cross-Coupling of Thiols With Aryl and Heteroaryl Iodides via Thiyl Radicals. *Journal of the American Chemical Society* **2016,** *138* (6), 1760-1763.

(3) Terrett, J. A.; Cuthbertson, J. D.; Shurtleff, V. W.; MacMillan, D. W. C., Switching on elusive organometallic mechanisms with photoredox catalysis. *Nature* **2015,** *524* (7565), 330-334.

(4) Xuan, J.; Zeng, T.-T.; Chen, J.-R.; Lu, L.-Q.; Xiao, W.-J., Room Temperature C-P Bond Formation Enabled by Merging Nickel Catalysis and Visible-Light-Induced Photoredox Catalysis. *Chemistry – A European Journal* **2015,** *21* (13), 4962-4965.

(5) Zhu, C.; Yue, H.; Jia, J.; Rueping, M., Nickel-Catalyzed C-Heteroatom Cross-Coupling Reactions under Mild Conditions via Facilitated Reductive Elimination. *Angewandte Chemie International Edition* **2021,** *60* (33), 17810-17831.

(6) Escobar, R. A.; Johannes, J. W., A Unified and Practical Method for Carbon–Heteroatom Cross-Coupling using Nickel/Photo Dual Catalysis. *Chemistry – A European Journal* **2020,** *26* (23), 5168-5173.

(7) Gravatt, C. S.; Johannes, J. W.; King, E. R.; Ghosh, A. Photoredox-Mediated, Nickel-Catalyzed Trifluoromethylation of Aryl and Heteroaryl Iodides. *Journal of Organic Chemistry* **2022**, *87* (14), 8921-8927.

(8) Candish, L.; Collins, K. D.; Cook, G. C.; Douglas, J. J.; Gómez-Suárez, A.; Jolit, A.; Keess, S., Photocatalysis in the Life Science Industry. *Chemical Reviews* **2022,** *122* (2), 2907-2980.

(9) Roughley, S. D.; Jordan, A. M., The Medicinal Chemist's Toolbox: An Analysis of Reactions Used in the Pursuit of Drug Candidates. *Journal of Medicinal Chemistry* **2011,** *54* (10), 3451-3479.

(10) Kudisch, M.; Lim, C.-H.; Thordarson, P.; Miyake, G. M., Energy Transfer to Ni-Amine Complexes in Dual Catalytic, Light-Driven C–N Cross-Coupling Reactions. *Journal of the American Chemical Society* **2019,** *141* (49), 19479-19486.

(11) Tian, L.; Till, N. A.; Kudisch, B.; MacMillan, D. W. C.; Scholes, G. D., Transient Absorption Spectroscopy Offers Mechanistic Insights for an Iridium/Nickel-Catalyzed C–O Coupling. *Journal of the American Chemical Society* **2020,** *142* (10), 4555-4559.

(12) Barman, K.; Edwards, M. A.; Hickey, D. P.; Sandford, C.; Qiu, Y.; Gao, R.; Minteer, S. D.; White, H. S., Electrochemical Reduction of $[Ni(Mebpy)_3]^{2+}$: Elucidation of the Redox Mechanism by Cyclic Voltammetry and Steady-State Voltammetry in Low Ionic Strength Solutions. *ChemElectroChem* **2020,** *7* (6), 1473-1479.

(13) Qin, Y.; Sun, R.; Gianoulis, N. P.; Nocera, D. G., Photoredox Nickel-Catalyzed C–S Cross-Coupling: Mechanism, Kinetics, and Generalization. *Journal of the American Chemical Society* **2021,** *143* (4), 2005-2015.

(14) Sun, R.; Qin, Y.; Ruccolo, S.; Schnedermann, C.; Costentin, C.; Nocera, D. G., Elucidation of a Redox-Mediated Reaction Cycle for Nickel-Catalyzed Cross Coupling. *Journal of the American Chemical Society* **2019,** *141* (1), 89-93.

(15) Till, N. A.; Tian, L.; Dong, Z.; Scholes, G. D.; MacMillan, D. W. C., Mechanistic Analysis of Metallaphotoredox C–N Coupling: Photocatalysis Initiates and Perpetuates Ni(I)/Ni(III) Coupling Activity. *Journal of the American Chemical Society* **2020,** *142* (37), 15830-15841.

(16) Kancherla, R.; Muralirajan, K.; Maity, B.; Karuthedath, S.; Kumar, G. S.; Laquai, F.; Cavallo, L.; Rueping, M., Mechanistic insights into photochemical nickel-catalyzed cross-couplings enabled by energy transfer. *Nature Communications* **2022,** *13* (1), 2737.

(17) Ren, H.; Li, G.-F.; Zhu, B.; Lv, X.-D.; Yao, L.-S.; Wang, X.-L.; Su, Z.-M.; Guan, W., How Does Iridium(III) Photocatalyst Regulate Nickel(II) Catalyst in Metallaphotoredox-Catalyzed C–S Cross-Coupling? Theoretical and Experimental Insights. *ACS Catalysis* **2019,** *9* (5), 3858-3865.

(18) Zhu, B.; Yan, L.-K.; Geng, Y.; Ren, H.; Guan, W.; Su, Z.-M., IrIII/NiII-Metallaphotoredox catalysis: the oxidation state modulation mechanism versus the radical mechanism. *Chemical Communications* **2018,** *54* (47), 5968-5971.

(19) Maity, B.; Zhu, C.; Yue, H.; Huang, L.; Harb, M.; Minenkov, Y.; Rueping, M.; Cavallo, L., Mechanistic Insight into the Photoredox-Nickel-HAT Triple Catalyzed Arylation and Alkylation of α-Amino Csp^3–H Bonds. *Journal of the American Chemical Society* **2020,** *142* (40), 16942-16952.

(20) Yu-Jiao Dong, B. Z., Yun Geng, Zhi-Wen Zhao, Zhong-Min Su, Wei Guan, Radical Mechanism of IrIII/NiII-Metallaphotoredox-Catalyzed $C(sp^3)$–H Functionalization Triggered by Proton-Coupled Electron Transfer: Theoretical Insight. *Chinese Chemical Society Chemistry* **2021,** *3*, 1456-1467.

(21) Zhou, S.; Lv, K.; Fu, R.; Zhu, C.; Bao, X., Nickel/Photoredox Dual Catalytic Cross-Coupling of Alkyl and Amidyl Radicals to Construct $C(sp^3)$–N Bonds. *ACS Catalysis* **2021,** *11* (9), 5026-5034.

(22) Kandoth, N.; Pérez Hernández, J.; Palomares, E.; Lloret-Fillol, J., Mechanisms of photoredox catalysts: the role of optical spectroscopy. *Sustainable Energy & Fuels* **2021,** *5* (3), 638-665.

(23) Arias-Rotondo, D. M.; McCusker, J. K., The photophysics of photoredox catalysis: a roadmap for catalyst design. *Chemical Society Reviews* **2016,** *45* (21), 5803-5820.

(24) Sandford, C.; Edwards, M. A.; Klunder, K. J.; Hickey, D. P.; Li, M.; Barman, K.; Sigman, M. S.; White, H. S.; Minteer, S. D., A synthetic chemist's guide to electroanalytical tools for studying reaction mechanisms. *Chemical Science* **2019,** *10* (26), 6404-6422.

(25) Vander Griend, D. A.; Bediako, D. K.; DeVries, M. J.; DeJong, N. A.; Heeringa, L. P., Detailed Spectroscopic, Thermodynamic, and Kinetic Characterization of Nickel(II) Complexes with 2,2'-Bipyridine and 1,10-Phenanthroline Attained via Equilibrium-Restricted Factor Analysis. *Inorganic Chemistry* **2008,** *47* (2), 656-662.

(26) Na, H.; Mirica, L. M., Deciphering the mechanism of the Ni-photocatalyzed C–O cross-coupling reaction using a tridentate pyridinophane ligand. *Nature Communications* **2022,** *13* (1), 1313.

(27) Goodgame, D. M. L.; Goodgame, M.; Cotton, F. A., Electronic Spectra of Some Tetrahedral Nickel(II) Complexes. *Journal of the American Chemical Society* **1961,** *83* (20), 4161-4167.

(28) Howe, E. N. W.; Bhadbhade, M.; Thordarson, P., Cooperativity and Complexity in the Binding of Anions and Cations to a Tetratopic Ion-Pair Host. *Journal of the American Chemical Society* **2014,** *136* (20), 7505-7516.

(29) Qiu, J.; Song, B.; Li, X.; Cozzolino, A. F., Solution and gas phase evidence of anion binding through the secondary bonding interactions of a bidentate bis-antimony(iii) anion receptor. *Physical Chemistry Chemical Physics* **2018,** *20* (1), 46-50.

(30) Thordarson, P., Determining association constants from titration experiments in supramolecular chemistry. *Chemical Society Reviews* **2011,** *40* (3), 1305-1323.

(31) Brynn Hibbert, D.; Thordarson, P., The death of the Job plot, transparency, open science and online tools, uncertainty estimation methods and other developments in supramolecular

chemistry data analysis. *Chemical Communications* **2016,** *52* (87), 12792-12805.

(32) Rivas Marquina, A.; Movilla, F.; Sanchez Montilva, O. C.; Rentschler, E.; Carrella, L.; Albores, P.; Di Salvo, F., Nickel(II) complexes based on l-amino-acid-derived ligands: synthesis, characterization and study of the role of the supramolecular structure in carbon dioxide capture. *Acta Crystallographica Section B* **2020,** *76* (5), 825-838.

(33) Kulakova, A. N.; Bilyachenko, A. N.; Korlyukov, A. A.; Levitsky, M. M.; Long, J.; Guari, Y.; Larionova, J., Novel carbonate/pyridine tetranuclear nickel complex, exhibiting slow relaxation of the magnetization. *Journal of Organometallic Chemistry* **2021,** *942*, 121815.

(34) Newell, R.; Appel, A.; DuBois, D. L.; Rakowski DuBois, M., Studies of Bicarbonate Binding by Dinuclear and Mononuclear Ni(II) Complexes. *Inorganic Chemistry* **2005,** *44* (2), 365-373.

(35) Till, N. A.; Oh, S.; MacMillan, D. W. C.; Bird, M. J., The Application of Pulse Radiolysis to the Study of Ni(I) Intermediates in Ni-Catalyzed Cross-Coupling Reactions. *Journal of the American Chemical Society* **2021,** *143* (25), 9332-9337.

(36) Du, Y.; Pearson, R. M.; Lim, C.-H.; Sartor, S. M.; Ryan, M. D.; Yang, H.; Damrauer, N. H.; Miyake, G. M., Strongly Reducing, Visible-Light Organic Photoredox Catalysts as Sustainable Alternatives to Precious Metals. *Chemistry – A European Journal* **2017,** *23* (46), 10962-10968.

(37) Sartor, S. M.; McCarthy, B. G.; Pearson, R. M.; Miyake, G. M.; Damrauer, N. H., Exploiting Charge-Transfer States for Maximizing Intersystem Crossing Yields in Organic Photoredox Catalysts. *Journal of the American Chemical Society* **2018,** *140* (14), 4778-4781.

(38) Lattke, Y. M.; Corbin, D. A.; Sartor, S. M.; McCarthy, B. G.; Miyake, G. M.; Damrauer, N. H., Interrogation of O-ATRP Activation Conducted by Singlet and Triplet Excited States of Phenoxazine Photocatalysts. *The Journal of Physical Chemistry A* **2021,** *125* (15), 3109-3121.

(39) Cagan, D. A.; Bím, D.; Silva, B.; Kazmierczak, N. P.; McNicholas, B. J.; Hadt, R. G., Elucidating the Mechanism of Excited-State Bond Homolysis in Nickel–Bipyridine Photoredox Catalysts. *Journal of the American Chemical Society* **2022,** *144* (14), 6516-6531.

(40) Ting, S. I.; Williams, W. L.; Doyle, A. G., Oxidative Addition of Aryl Halides to a Ni(I)-Bipyridine Complex. *Journal of the American Chemical Society* **2022,** *144* (12), 5575-5582.

(41) Yang, L.; Huang, Z.; Li, G.; Zhang, W.; Cao, R.; Wang, C.; Xiao, J.; Xue, D., Synthesis of Phenols: Organophotoredox/Nickel Dual Catalytic Hydroxylation of Aryl Halides with Water. *Angewandte Chemie International Edition* **2018,** *57* (7), 1968-1972.

(42) Troian-Gautier, L.; Turlington, M. D.; Wehlin, S. A. M.; Maurer, A. B.; Brady, M. D.; Swords, W. B.; Meyer, G. J., Halide Photoredox Chemistry. *Chemical Reviews* **2019**, *119* (7), 4628-4683.

(43) Dorsheimer, J. R.; Ashley, M. A.; Rovis, T., Dual Nickel/Photoredox-Catalyzed Deaminative Cross-Coupling of Sterically Hindered Primary Amines. *Journal of the American Chemical Society* **2021,** *143* (46), 19294-19299.

(44) Wang, D.; Xu, T., A Pivotal Role of Chloride Ion on Nickel-Catalyzed Enantioselective Reductive Cross-Coupling to Perfluoroalkylated Boronate Esters. *ACS Catalysis* **2021,** *11* (20), 12469-12475.

(45) Earley, J. D.; Zieleniewska, A.; Ripberger, H. H.; Shin, N. Y.; Lazorski, M. S.; Mast, Z. J.; Sayre, H. J.; McCusker, J. K.; Scholes, G. D.; Knowles, R. R.; Reid, O. G.; Rumbles, G., Ion-pair reorganization regulates reactivity in photoredox catalysts. *Nature Chemistry* **2022,** *14* (7), 746-753.

Insert Table of Contents artwork here